

# Gravitational-Wave Detection and Astrophysics with Pulsar Timing Arrays

S. Burke-Spolaor<sup>1</sup>

*National Radio Astronomy Observatory, PO Box O, 1003 Lopezville Rd, Socorro, NM 87801-0387, USA*  
 sspolaor@nrao.edu

## ABSTRACT

We have begun an exciting era for gravitational wave detection, as several world-leading experiments are breaching the threshold of anticipated signal strengths. Pulsar timing arrays (PTAs) are pan-Galactic gravitational wave detectors that are already cutting into the expected strength of gravitational waves from cosmic strings and binary supermassive black holes in the nHz- $\mu$ Hz gravitational wave band. These limits are leading to constraints on the evolutionary state of the Universe. Here, we provide a broad review of this field, from how pulsars are used as tools for detection, to astrophysical sources of uncertainty in the signals PTAs aim to see, to the primary current challenge areas for PTA work. This review aims to provide an up-to-date reference point for new parties interested in the field of gravitational wave detection via pulsar timing.

*Subject headings:* pulsars: general

## 1. Introduction

The discovery of pulsars in 1968 initiated the flourishing field of pulsar astronomy, opening up the use of pulsars as tools to perform a vast range of experiments. The beams of light emitted from pulsars' magnetic poles mark their rotational phase at each turn. Coupled with their exceptional rotational stability, most pulsars are massive, moving, precisely ticking test masses: an ideal relativity tester.

One of the leading uses of pulsars is in “Pulsar Timing Arrays” (PTAs), which aim to detect gravitational radiation via a pan-Galactic detector. The basic premise of the PTA is to detect variations in the arrival phases of a pulsar's tick, and search for correlations in these variations in a set of pulsars distributed across the sky. This method of gravitational wave (GW) detection is both competitive and complementary to other experiments pursuing the first direct detection of GWs (Fig. 1).

This review seeks to provide an accessible

broad-strokes outline of the background, current state, and major efforts of gravitational wave detection with PTAs, for anyone new to, or wishing to enter, this field.

## 2. Basics

### 2.1. Timing data and GW frequency range

The basic data product of PTAs are “timing residuals”, of which each data point is a pulse arrival time minus the pulse's predicted arrival time. Each timing data point is built from a long observation of each pulsar—typically averaged over tens of thousands of rotations—long enough so that its profile is relatively stable and of a sufficiently high signal-to-noise ratio (Fig. 2; see also §4.1). Typical durations are approximately 0.5–1 h with current telescopes (Manchester et al. 2013; McLaughlin 2013; Kramer & Champion 2013). The GW frequency sensitivity is set by the observing cadence,  $C$ , i.e. a pulsar typically gets one datum every  $\sim 3$  weeks, and the total span of data,  $T$ , which can right now in principle be up to  $\sim 30$  years, as precision timing was first done in the 1980s (Backer,

---

<sup>1</sup>Jansky Fellow

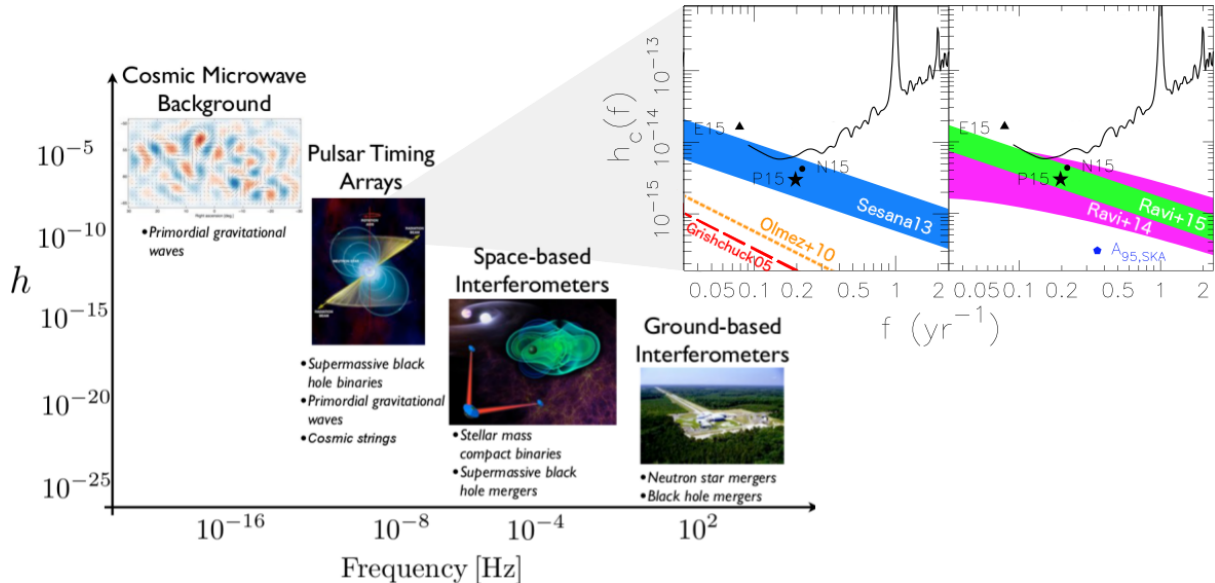


Fig. 1.— A conceptual strain spectrum, showing the complementarity of GW detection techniques adapted from a figure by NANOGrav. The anticipated sources, listed for each frequency range, are also complementary. The inset figure shows an enhanced view of the predicted GWB and limits in the PTA band (adapted and updated from Shannon et al. 2015). The 68% uncertainty range of several BSMBH simulations are indicated (filled curves), as are representative spectra from inflationary GWs (red long-dashed) and cosmic strings (orange short-dashed). The best limits are also shown; points are from PPTA, NANOGrav, and the EPTA (Shannon et al. 2015; Arzoumanian et al. 2015a; Lentati et al. 2015, respectively); the curve is from PPTA (Shannon et al. 2015).

Kulkarni & Taylor 1983). Hence,  $T^{-1} \lesssim f \lesssim C^{-1}$  gives the classically quoted nHz– $\mu$ Hz sensitivity.

The predicted arrival time of a pulse is built from a model of the pulsar’s spin evolution. Because intrinsic pulsar spin and binary properties are not directly measurable, these are solved for by the timing process itself: with any new data, the pulsar parameters are re-fit and a more accurate timing model is obtained before any GW search can be performed. Some GW power may be absorbed by this process (Fig. 3). Fortunately, most intrinsic parameters vary from pulsar to pulsar, hence PTAs only suffer significant sensitivity losses at frequencies of 1 year and 0.5 year due to positional and parallax fitting, and at the lowest frequencies to period ( $\propto t$ ) and period derivative fitting ( $\propto t^2$ ).

A general figure of merit for pulsar timing precision is the root mean squared of the timing residuals,  $\sigma_n$ , which for the best pulsars is  $\lesssim 100$  ns, however is more typically  $\lesssim 1 \mu$ s for pulsars included in current PTAs.

## 2.2. Gravitational waves’ effect on pulsar signals

Gravitational radiation is a propagating change in the curvature of spacetime, parameterized by the dimensionless strain,  $h$ . Because we expect no Galactic source of gravitational waves to be large enough to be detected by PTAs,<sup>1</sup> throughout this review we consider only GWs in the far-field regime: that is, well outside of our galaxy. From any GW source there is a path difference, and hence travel time delay, between the source-Earth path and the source-pulsar-Earth path. For a far-field source, a GW’s appearance in timing residuals at time  $t$  has been shown to be the difference  $\Delta h_{+, \times} = h_{+, \times}^p - h_{+, \times}^E$  between the GW’s distortion of Earth’s space-time (“Earth term,”  $h_{+, \times}^E(t)$ ) and the GW’s distortion of pulsar space-time (“pulsar term,”  $h_{+, \times}^p(t - d/c)$  for a pulsar of distance  $d$ ). The plus and cross represent the two polarization states possible in general relativity.

<sup>1</sup>Except, perhaps, for intermediate-mass black hole binaries in our Galaxy’s globular clusters, (e.g. Jenet, Creighton & Lommen 2005).

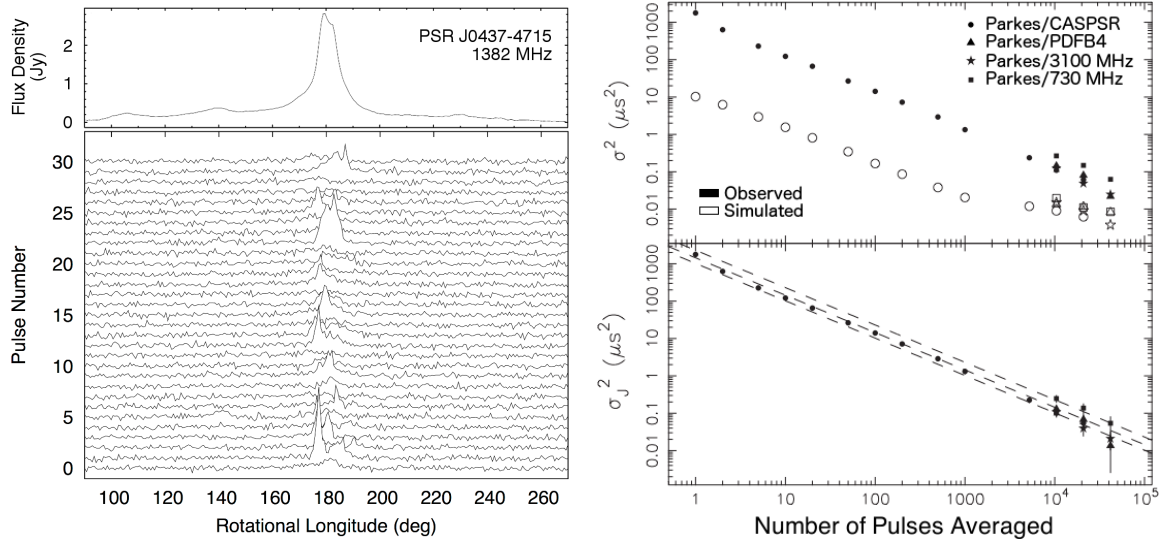


Fig. 2.— Each rotation of a pulsar can present a vastly different profile (“jitter”), yet on timescales of  $\gtrsim 1$  h the rotationally averaged profile is stable. For this reason, each timing residual data point is usually made up of an  $\sim 1$  h pulsar observation. On the left, we show 30 single pulses from one of the best-timed pulsars. The top panel shows its stable profile after 1 h of integration. The right panel, from Shannon et al. (2014), shows the RMS residual level vs. number of pulses contributing to the integrated profile for real and simulated data (top), and the quadrature subtraction of these (bottom).

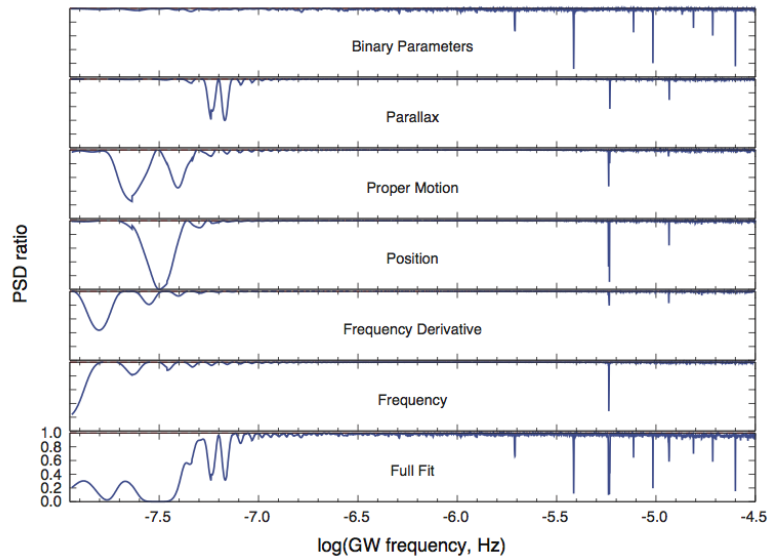


Fig. 3.— From Cutler et al. (2014): GW power absorbed by parameter fitting for PSR J0613-0200. The ordinate is the ratio of power spectral density for residuals before and after parameter fitting. Only the indicated parameters were fit. Frequencies  $f \sim 1 \text{ year}^{-1}$  are fully absorbed by pulsar position fits, thus are not detectable by PTAs; this corresponds to the  $1 \text{ year}^{-1}$  sensitivity spike of Fig. 1. PTAs are also decreasingly sensitive as  $f \rightarrow T^{-1}$ , which in this simulation was just below the window shown here. (Blandford, Romani & Narayan 1984; see also Cordes (2013) for an excellent discussion of GW sensitivity limits due to intrinsic pulsar noise and parameter fitting. Copyright (2014) by The American Physical Society

As in Detweiler (1979), we can phrase the GW-induced residual signal as a shift in the pulsar spin frequency,  $\nu_0$ .<sup>2</sup> For a GW travelling in cartesian coordinates along the positive  $z$  direction, the induced frequency shift depends on a pulsar’s direction cosines  $\alpha$ ,  $\beta$ , and  $\gamma$  to the  $x$ ,  $y$ , and  $z$  axes. The coefficients in front of the cross and plus terms in the equation below define the quadrupolar “antenna pattern” expected to be seen from GWs when correlating the residuals of pulsars with different direction cosines. The frequency shift is given by

$$\frac{\nu_0 - \nu(t)}{\nu_0} = \frac{\alpha^2 - \beta^2}{2(1 + \gamma)} \Delta h_+(t) + \frac{\alpha\beta}{1 + \gamma} \Delta h_\times(t). \quad (1)$$

Finally, the residuals induced by the GW are given by the integral over time of Eq. 1:

$$R(t) = \int_0^t \frac{\nu_0 - \nu(t')}{\nu_0} \delta t'. \quad (2)$$

Fig 4 shows examples of  $R(t)$  for several source classes.

### 2.3. Leading PTA experiments

The sensitivity scaling of PTAs depends on the type of target signal, however the factors contributing are minimizing the pulsars’  $\sigma_n$  values, and the presence of “intrinsic red noise” in a pulsar’s timing residuals (§4.1), while maximizing the total number of pulsars, the observing cadence, and the total data span. The most sensitive PTA experiments optimize these aspects. In the past decade, there has been a push towards large, coordinated pulsar timing programs. We will describe the leading programs here in brief; please see the noted publications for details.

**The North American Nanohertz Observatory for Gravitational Waves** (NANOGrav)<sup>3</sup> has been running for  $\sim 1$  decade (Arzoumanian et al. 2015b), and is currently using sensitive wide-bandwidth receivers at Green Bank and Arecibo telescopes to time 49 pulsars (and counting; P. Demorest, private comm.), each observed at least at two radio frequencies between 327 MHz and

2.3 GHz. The reason for bi-frequency timing is to mitigate effects of the inter-stellar medium on the timing residuals; this is discussed further in §4.1. Arecibo telescope has the benefit of the largest collecting area—and largest sensitivity—of all the world’s telescopes, although its size inhibits its sky coverage, so that it only may observe 27 of the current NANOGrav pulsars.

**The European Pulsar Timing Array** (EPTA)<sup>4</sup> is a collaboration which uses five telescopes across Europe—Effelsberg, Lovell, Nançay, Sardinia, and Westerbork—to separately time a primary set of 41 pulsars at various frequency pairs between 300 MHz and 3.5 GHz (Kramer & Champion 2013; Desvignes in prep.). The collaboration is also working to combine all telescope signals coherently in a “Large European Array for Pulsars,” which will effectively be a fully-steerable telescope with a collecting area equal to that of Arecibo (Kramer & Champion 2013). Because five telescopes contribute independently to EPTA data, it boasts the highest cadence of the three PTAs, effectively having one data point per pulsar each week.

**The Parkes Pulsar Timing Array** (PPTA)<sup>5</sup> times 25 pulsars using Parkes Observatory in Australia at frequencies of 600 MHz, 1.5 GHz, and 3 GHz. This experiment is unique due to the telescope’s position in the southern hemisphere; it can see a distinct set of pulsars not visible to the EPTA nor NANOGrav, which includes one of the best-timed pulsars in the sky, PSR J0437–4715 (Hobbs et al. 2010). The PPTA has continually boasted the best constraints on gravitational radiation.

Finally, the aptly-named **International Pulsar Timing Array** (IPTA)<sup>6</sup> represents the coordinated effort to combine data from the above three projects to reach the best possible sensitivity to GWs (Hobbs et al. 2010; Manchester & IPTA 2013; McLaughlin 2014). For its initial 2015 data release, the array contains a total of 49 pulsars (Verbiest et al. in prep). Note this number is not the sum of the above collaborations’ pulsars because the PTAs do not time mutually exclusive pulsars, and the 2015 IPTA data release does not contain pulsars that have been added to the con-

<sup>2</sup>Spin frequency is constant here, which is sufficiently true after correcting for the fitted pulsar spin derivative and parameters.

<sup>3</sup><http://nanograv.org/>

<sup>4</sup><http://www.epta.eu.org/>

<sup>5</sup><http://www.atnf.csiro.au/research/pulsar/ppta/>

<sup>6</sup><http://www.ipta4gw.org/>

stituent arrays in only the last few years. In addition to coordinating data and combined-PTA science, the IPTA hosts annual PTA science meetings around the world, and organizes related public efforts like PTA Mock Data Challenges (e.g. van Haasteren et al. 2013; Ellis, Siemens & Chamberlin 2012; Cornish 2012).

### 3. Upper Limits and Detection of GWs

There are four distinct “classes” of signals which might appear in the nHz- $\mu$ Hz GW band, with several astrophysical sources that can produce them. A simulated example of how each might appear in timing residuals is shown in Fig. 4.

Different techniques have been developed to place upper limits on each class of signal. However, for all classes, the only way to verify a detection is to demonstrate the expected quadrupolar signature, for instance via the so-called “Hellings and Downs curve,” which demonstrates the expected cross-correlation function for two pulsars as a function of their angular separation on the sky (Hellings & Downs 1983; Finn, Larson & Romano 2009).<sup>7</sup> For this reason, while upper limits can be placed using data from one pulsar, *at least three pulsars* must be used in an array to demonstrate that a GW has been *detected*.

#### 3.1. Stochastic Gravitational-Wave Background (GWB)

This describes a signal built from the ensemble contributions of discrete GW sources. It manifests as randomly varying strain fluctuations with a well-defined spectral distribution. The GWB’s spectrum, as a fractional contribution of the GWB to the energy density of the Universe in a logarithmic frequency interval, can be expressed (assuming a Freedman-Robertson-Walker universe) as

$$\Omega_{\text{gw}}(f) = \frac{2\pi^2}{3H_0^2} f^2 h_c(f)^2, \quad (3)$$

(e.g. Maggiore 2000), where  $H_0$  is the Hubble constant, and  $h_c(f)$  represents the “characteristic

<sup>7</sup>This curve has been shown to hold both for a stochastic background, and for a discrete source of GWs. However, the expected overlap reduction function may differ for non-general-relativistic theories of gravity (e.g. Chamberlin & Siemens 2012). The pulsar term (§2.2) will also cause scatter around the predicted curve.

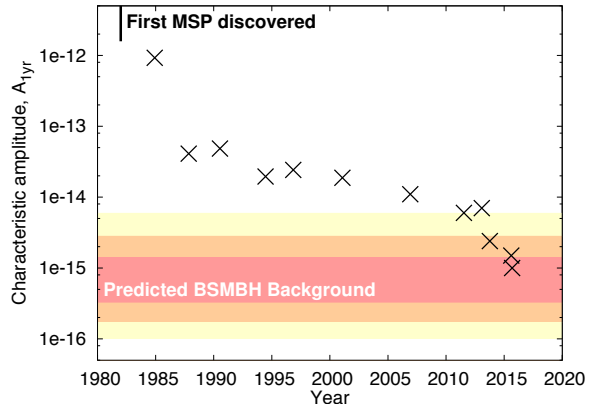


Fig. 5.— Upper limits on the power-law GWB for a spectral index  $\alpha = -2/3$ . Limits improved steadily after dedicated timing of millisecond pulsars commenced. The sudden drop after 2013 arises, most importantly, from optimized PTA experiments finally coming to fruition. The red, orange, and yellow ranges give the 68, 95 and 99.7% confidence intervals of the Sesana (2013b) model. References: Backer et al. (1982); Blandford, Romani & Narayan (1984); Rawley et al. (1987); Stinebring et al. (1990); Kaspi, Taylor & Ryba (1994); McHugh et al. (1996); Lommen (2001); Jenet et al. (2006); van Haasteren et al. (2011); Demorest et al. (2013); Shannon et al. (2013); Arzoumanian et al. (2015a); Shannon et al. (2015); Lentati et al. (2015)

strain spectrum,” which is built from the quadrature sum over the individual strains from a GW source population.

For a time, most predictions of the GWB parameterized the strain spectrum by a power law, such that the strength of the background can be characterized by an amplitude  $A_{1\text{yr}}$  for an index  $\alpha$ ,

$$h_c(f) = A_{1\text{yr}} \left( \frac{f}{1 \text{ yr}} \right)^\alpha. \quad (4)$$

Pulsar timing limits are often quoted in one of three ways: either the  $h_c$  or  $\Omega_{\text{gw}}$  limit at  $f$  where  $f \gtrsim T^{-1}$ , or as a limit on  $A_{1\text{yr}}$  for a specific  $\alpha$  value. The most sensitive limits are placed at  $f > T^{-1}$  because of signal absorption by pulsar fitting at  $f \lesssim T^{-1}$  (Fig. 3). Reporting an  $(A_{1\text{yr}}, \alpha)$  pair allows easy comparison between upper limits from different PTA experiments.

Current consensus is that the dominant GWB signal in the nanohertz waveband will be from binary supermassive black holes (BSMBHs; where

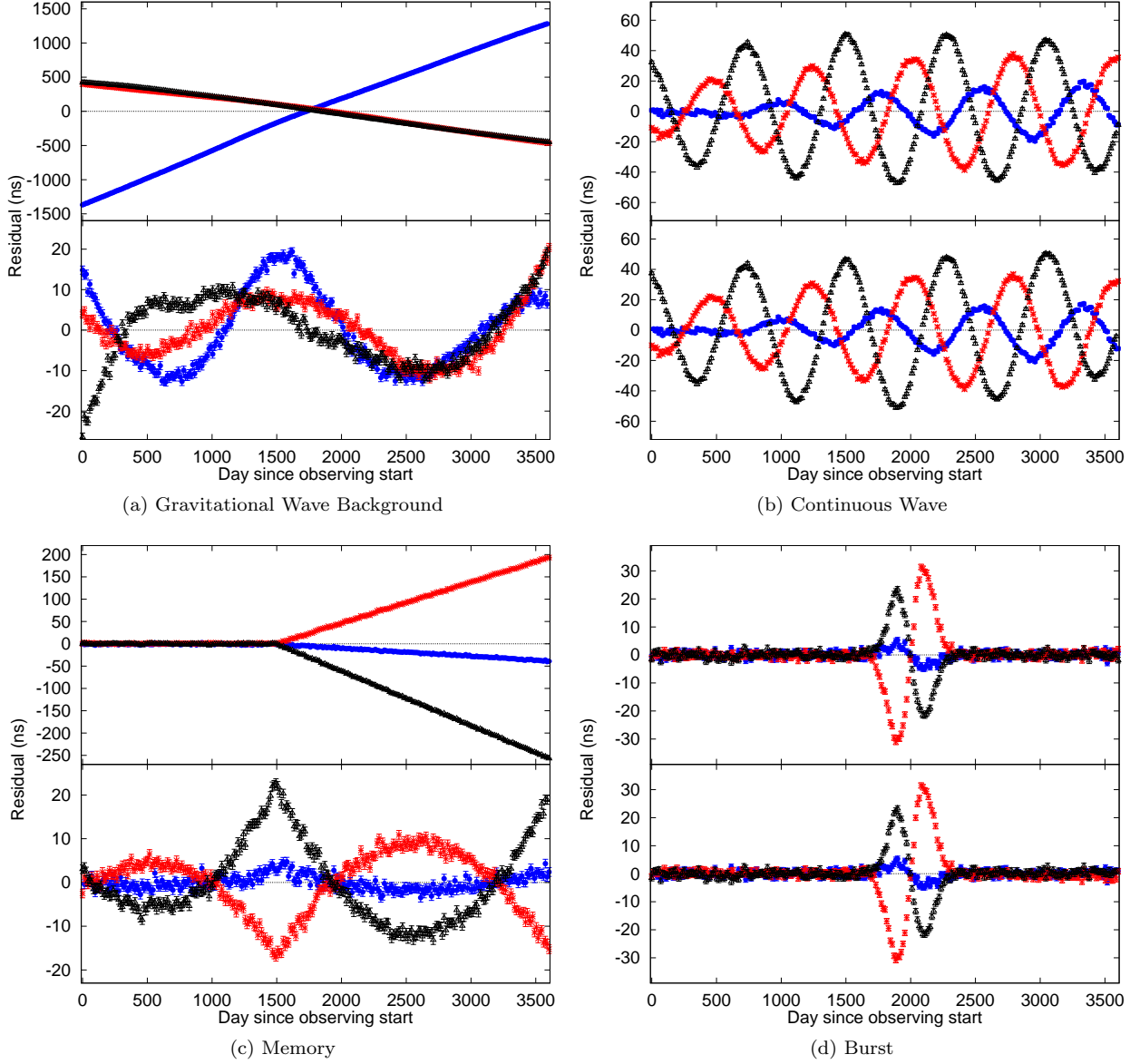


Fig. 4.— Examples of the four classes of GW signals predicted in the pulsar timing band. Each graphic shows the induced timing residuals before parameter fitting (top panel) and after fitting for pulsar spin period and period derivative (bottom panel), for simulated data from pulsars PSR J0437–4715 (red asterisks), J1012+5307 (blue dots), and J1713+0747 (black triangles) to demonstrate the expected quadrupolar signature. All discrete GW sources (b–d) were injected in the same sky location. In all simulated pulsar residuals,  $\sigma_n = 1$  ns of white noise and no red noise was injected. Panels are: (a) A GWB with  $h_c = 10^{-15}$  and  $\alpha = -2/3$ ; (b) A continuous wave from an equal-mass  $10^9 M_\odot$  BSMBH at redshift  $z = 0.01$ . The distortion from a perfect sinusoid is caused by the lower-frequency pulsar term. (c) A memory event of  $h = 5 \times 10^{-15}$ , whose wavefront passes the Earth on day 1500. (d) A burst source with an arbitrary waveform.

$\alpha = -2/3$  (Phinney 2001). See also §5), however predictions have also been made for cosmic strings ( $\alpha = -5/3, -7/6$ , or  $-1$  depending on the frequency range and kink vs. cusp signal; Damour & Vilenkin 2001; Ölmez, Mandic & Siemens 2010), and inflationary relic GWs ( $\alpha = -2$  to  $-0.5$  depending on the equation of state during the inflationary epoch, e.g. Grishchuk 2005). Other suggested sources of a GWB, such as primordial black holes (Bugaev & Klimai 2011) and QCD phase transitions (Caprini, Durrer & Siemens 2010), do not fit a power-law dependence for  $h_c$ . All predicted PTA backgrounds have greater power at low frequency. The result of this is a red-noise wander in the timing residuals that is correlated across different pulsars, as seen in Fig. 4a.

We will not review limit algorithms, however do encourage readers to read about frequentist approaches in e.g. Shannon et al. (2013); Ellis, Siemens & van Haasteren (2013). Bayesian inference is also increasingly used, e.g. van Haasteren et al. (2011); Ellis (2013); Lentati et al. (2015).

As of yet there has been no detection, however increasingly tight upper limits have been placed on the GWB. Upper limits to date for  $A_{1\text{yr}}$  and  $\alpha = -2/3$  are shown in Fig. 5, indicating a steady improvement with a drop in nearly an order of magnitude over the last decade. See also §5, and Figs. 1 and 10 for other views and further implications of PTA limits for the BSMBH population.

The best limits to date on other sources include **cosmic strings**,  $A_{1\text{yr}} < 6 \times 10^{-16}$  at  $\alpha = -7/6$  (Arzoumanian et al. 2015a). This limit’s interpretation depends heavily on a number of parameters, including string loop radius and the probability of two strings connecting; see e.g. Fig. 12 in Arzoumanian et al. (2015a). However, for the range of parameters assumed by Arzoumanian et al., they set a conservative upper limit on the string tension of  $G\mu < 3.3 \times 10^{-8}$ , which is four times more constraining than previously published limits. See also Lentati et al. (2015) for an excellent discussion of the impact of PTA limits on cosmic strings. Current limits also impact **inflationary GWs**,  $A_{1\text{yr}} < 8.1 \times 10^{-16}$  at  $\alpha = -1$ . Following the framework of Zhao (2011), this provides a limit on the Hubble parameter during the inflationary era of  $H_*/m_{\text{P}} < 1.6 \times 10^{-2} m_{\text{P}}$ , where  $m_{\text{P}}$  is the Planck mass (Arzoumanian et al. 2015a).

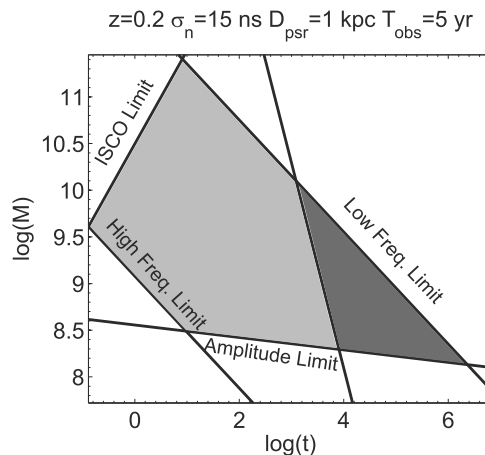


Fig. 6.— From Lee et al. (2011): The parameter space of BSMBHs detectable as CW sources by a representative PTA. The abscissa is  $\log(t_{\text{gw}})$  (Eq. 5) in years; the ordinate is the chirp mass in units of  $M_{\odot}$ . The “Amplitude Limit” depends on PTA sensitivity, and the “Low and High  $f$  Limits” bound the PTA GW band. “ISCO” is the inner-most stable circular orbit. Evolving and non-evolving binaries are light and dark grey, respectively. The dominantly detectable population is in the dark gray region, where we encounter smaller masses but much longer system lifetimes.

### 3.2. Continuous Waves (CW)

CWs are, as their name implies, continuous in time. The generation of bright CWs in the nHz– $\mu$ Hz GW band requires massive objects in a state of constant acceleration at lengths of decades; currently the only sources known to fit this requirement are BSMBHs whose orbit is gradually shrinking due to GW emission. If a binary in its rest frame is orbiting at a frequency  $f_{\text{br}}$ , a circular binary will emit GWs at a rest-frame frequency  $f_r = 2f_{\text{br}}$ , and an Earth-observed frequency  $f = 2f_{\text{br}}/(1+z)$ . Any eccentricity in the system will spread the observed GW power to higher harmonics of  $f$  (e.g. Enoki & Nagashima 2007). Thus, binaries of orbital periods in the range of weeks to decades will emit CWs in the PTA band. These systems spend more time at longer orbital periods, as per the timescale to coalescence given by a purely GW-driven orbital inspiral (Merritt & Milosavljević 2005):

$$t_{\text{gw}} = \frac{5}{256F(e)} \frac{c^5}{G^{5/3}} \frac{(m_1 + m_2)^{1/3}}{m_1 m_2} (\pi f_r)^{-8/3}, \quad (5)$$

where  $a$  is the semi-major axis of the system and  $m_1, m_2$  are the masses of the two black holes. Because of the time delay between the Earth and pulsar term can be several tens of thousands of years (see §2.1), there may be some evolution in the BSMBH between these two terms. This would cause two sinusoids of different phase and frequency to appear in each pulsar’s data stream: a low-frequency pulsar term and a higher-frequency Earth term, the latter of which would be the same in all pulsars in the PTA. A source with a significant difference between Earth and pulsar term is said to be “evolving”. Figure 6 indicates the parameters defining what BSMBH systems would be expected to emit CWs detectable by a typical PTA experiment. The signal from a weakly evolving source is shown in Fig. 4b.

The GWB is generally expected to be the dominant signal in the PTA band, however numerous studies have indicated that CW signals from BSMBHs will be resolvable above the stochastic background (e.g. Sesana, Vecchio & Volonteri 2009; Boyle & Pen 2012; Rosado, Sesana & Gair 2015). A number of both targeted and blind searches have been performed for CWs from circular BSMBHs. These searches are able to translate GW upper limits into statements on what

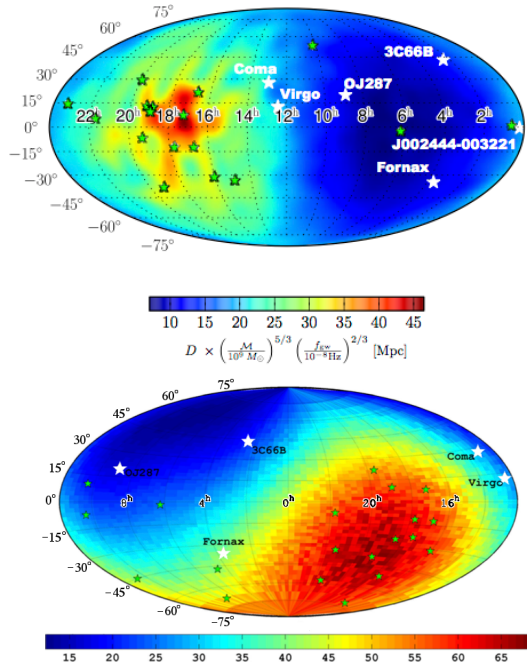


Fig. 7.— From NANOGrav (top, Arzoumanian et al. 2014), and PPTA (bottom, Zhu et al. 2014): At the time of those publications, the respective PTAs were sensitive to SMBHs out to the color-coded distance  $D$ , normalized here for an equal-mass  $10^9 M_{\odot}$  binary with  $f = 10^{-8}$  Hz. Note the 12 h R.A. shift between the panels. The difference in sky sensitivity distribution is caused by the different positions of the pulsars in the arrays (small green stars).



BSMBHs must not exist out to some distance at a given mass, mass ratio, and orbital frequency. Targeted limits have been placed on binaries in SgrA\* and nearby galaxies (Lommen & Backer 2001), and perhaps the most noteworthy targeted limit was that on GWs from 3C66B, which had been suggested via an observation of elliptical motion of its radio core to be a BSMBH system (Sudou et al. 2003). The implied system parameters for 3C66B were quickly ruled out because the corresponding GW signal would have been detected by the PPTA with great significance (Jenet et al. 2004). To date the most sensitive upper limits from blind BSMBH searches are shown in Fig. 7, along with several nearby clusters and candidate BSMBHs.

### 3.3. Memory Events

GW memory describes an event which causes a static (non-oscillating), propagating change in strain. This is expected to occur upon the coalescence of a BSMBH, or from a BSMBH on a hyperbolic orbit (Favata 2009a,b). Physically, GW memory passing Earth can be thought of as a permanent displacement of the local space-time following a rapid ( $\ll 1$  day) ramp in the local metric as the wave passes. The ramp itself is not detectable by pulsar timing, but the sudden change in Earth’s space-time induces a small change observed in the pulsar period, which results in a gradual drift of timing residuals away from null because the previous timing model is rendered inaccurate (Fig. 4c).

The memory signal would also appear in the pulsar term, however it would not be coincident in time with other pulsars: the pulsar term is detected at a time  $(d/c)(1 + \cos(\theta))$  later than the correlated Earth term, where  $\theta$  is the separation angle between the pulsar and the GW source as seen from the Earth.

Predictive simulations have found that PTAs are highly unlikely to detect GW memory, largely due to the extreme rarity of bright events (Seto 2009; van Haasteren & Levin 2010; Cordes & Jenet 2012). Still, techniques to search for memory in PTAs have been developed (Madison, Cordes & Chatterjee 2014) and limits have been placed: most recently, results from PPTA and NANOGrav bounded the event rate of events with strain  $h > 10^{13}$  to be  $< 0.75 \text{ yr}^{-1}$  and  $< 1.5 \text{ yr}^{-1}$ , respectively

(Wang et al. 2015; Arzoumanian et al. 2015c). However, PTA sensitivity is still several orders of magnitude above the predicted memory strain signals (Wang et al. 2015).

### 3.4. Transient Bursts

For PTAs, a transient or burst source is defined as an event whose duration  $\tau \ll T$ ; and of course it would only be detectable if  $\tau \gtrsim 1$  day, such that the residuals of multiple pulsars could be observed to be affected by the burst signal.

Bursts may arise from cusps and kinks in cosmic strings (Damour & Vilenkin 2001), or from encounters of compact objects with a SMBH, including SMBHs in an unbound orbit (Finn & Lommen 2010). While several methodologies for burst detection via PTAs have been developed Finn & Lommen (2010); Deng (2014); Zhu et al. (2015), as of yet none have been published which apply the techniques to real (non-simulated) PTA data.

## 4. Current discussions and challenges in pulsar timing

Here we touch on major efforts that aim to maximize PTA sensitivity and understand the future of GW detection with PTAs. One further major effort is in the modelling of BSMBH populations; however, this is covered in detail in §5.

### 4.1. Conquering timing noise

The RMS level  $\sigma_n$  of timing residuals is critically important to PTA sensitivity, and for many pulsars encompasses both a red (increasing at low power) and white (gaussian) noise component. Examples of timing residuals dominated by different types of noise can be seen in Fig. 8.

Some noise sources are surmountable. For most pulsars observed with current telescopes, the dominant white noise contribution comes from the low signal-to-noise (S/N) of the observed profile used to make a timing residual. Such pulsars are “S/N limited”. This is perhaps the most (conceptually) easy noise to overcome, simply requiring a more sensitive radio telescope, which would involve recording at higher bandwidth ( $S/N \propto \sqrt{B}$ ), better cooling one’s receivers, or having greater collecting area ( $S/N \propto A$ ). Improvements from higher bandwidth are visible in PSR J0613–0200 in

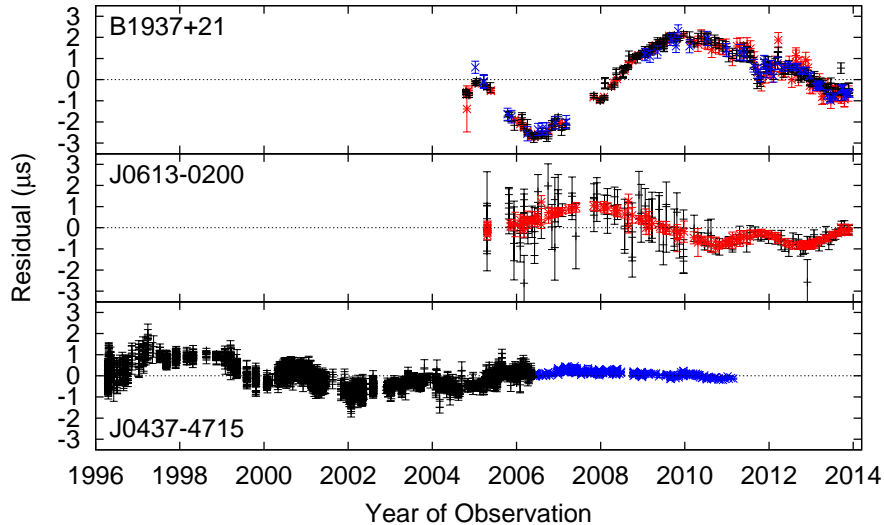


Fig. 8.— Timing residuals from three pulsars, exhibiting different kinds of noise: intrinsic red timing noise (PSR B1937+21), a S/N limited pulsar with a mild level of red timing noise (PSR J0613–0200), and a pulsar exhibiting uncorrected dispersion measure variations (PSR J0437–4715 prior to 2007 was only observed at a single frequency, thus is not corrected for this effect prior to that date). Colors indicate the radio frequency of the observation:  $\sim 1$  GHz (black),  $\sim 800$  MHz (red), and  $\sim 3$  GHz (blue). Data are from NANOGrav (PSRs B1937+21, J0613–0200: Arzoumanian et al. 2015b) and the PPTA (PSR J0437–4715: Manchester et al. 2013). See §4.1 for discussion.

Fig. 8; in 2010, the new “GUPPI” instrument was installed at Greenbank telescope, which raised the bandwidth that the instrument could observe by more than a factor of 10. As discussed later, however, even S/N improvements cannot overcome intrinsic pulse “jitter.”

One of the main sources of red noise in timing residuals comes from turbulence in the interstellar medium (ISM). As the pulsar, ISM, and Earth itself move, we see pulsars through a continuously changing line-of-sight through the ISM, and the resulting electron density variance creates a wandering delay in the pulse’s arrival at Earth (“dispersion,” e. g. Lorimer & Kramer 2004). Fortunately, this effect is radio-frequency-dependent and can be directly measured using at least two broadly-separated radio bands; this is the primary reason for multi-frequency observations noted in §2.3. For PSR J0437–4715, the PPTA only commenced multi-frequency observations in 2006; the strong red signal diminishes thereafter due to the correction of dispersion variations (Fig. 8). The remaining low-level signal is likely due to intrinsic timing noise in this pulsar.

Not all pulsars appear to be limited by extrinsic noise sources: for instance greater receiver bandwidth after the year 2010, and hence greater S/N, did not improve PSR B1937+21. All three pulsars shown in Fig. 8 retain some red noise signal despite dispersion corrections. The remaining noise is considered intrinsic noise, which is likely due to short (“jitter,” Fig. 2) and long-term rotational instabilities in the pulsar itself (Cordes 2013).

This is a critical notion for the long-term sensitivity of pulsar timing and in designing future experiments: wherein even using ideal telescopes with maximized sensitivity, a fundamental instability in each of our pulsars could be a basic impediment to GW detection. The pulsar emission mechanism is a vast field of pursuit and it seems that intrinsic pulsar noise is non-deterministic (Rickett 1975). Thus, a number of current studies have aimed to find practical ways to side-step jitter, for instance creating timing residuals using pulse profiles made up of only high S/N rotations (Osłowski et al. 2011; Shannon et al. 2014). However, so far the only tried and true way to mitigate jitter is to integrate over a large num-

ber of pulses ( $\sigma_n \propto N^{-1/2}$ ; Shannon & Cordes 2012). Attempts at GW detection/limits, particularly those in pursuit of the GWB, must also account for intrinsic red signals present in pulsars (e.g. by noise modelling, by selecting only white-noise-dominated pulsars, and by “pre-whitening” schemes; Shannon et al. 2013).

Finally, it is possible that other issues, such as time-transfer from atomic clocks or our knowledge of solar system ephemerides, will form a fundamental sensitivity limit for PTAs (Jenet, Armstrong & Tinto 2011). However, because of constant ongoing improvements in terrestrial clock precision and solar system ephemerides, at least in the coming decades these sources of noise are not expected to dominate timing error.

#### 4.2. The search for new pulsars

Finding many pulsars that can be timed to low  $\sigma_n$  is another important part of increasing PTA sensitivity. Only a few low- $\sigma_n$  pulsars ( $\lesssim 200$  ns) contribute significantly to the PTAs in §2.3 (e.g. only 6/20 pulsars contributed to the limit of Shannon et al. 2013). Millisecond pulsars (MSPs)—pulsars with rotational frequencies of hundreds of Hz—are the only pulsars stable enough for PTA use, and there are ongoing world-wide efforts to find and time these to determine their suitability for PTAs (e.g. Lynch et al. 2013; Barr et al. 2013; Bates et al. 2015). This has turned up around 20–30 new millisecond pulsars *per year* in the past 6 years, although less than around five of these per year have been found suitable for PTA use, with  $\sigma_n \lesssim 1 \mu\text{s}$  (McLaughlin 2014). However, there remain many potential MSP goldmines. It is estimated that there are  $\sim 10^4$  MSPs in the galaxy compared to the several hundred currently known (Swiggum et al. 2014). This wealth of MSPs will become readily observable with future telescopes with wide bandwidth and large collecting area, like the Square Kilometre Array (SKA; Janssen et al. 2015) and the Five hundred meter Aperture Spherical Telescope (FAST; Hobbs et al. 2014). If intrinsic timing noise—particularly red noise—is unsolvable, adding pulsars to one’s array is the best way to improve sensitivity to GWs.

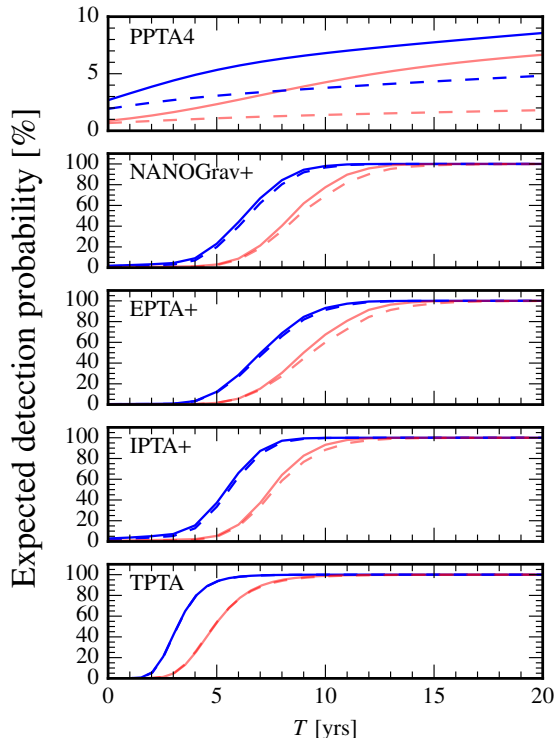


Fig. 9.— From Taylor et al. (2015a): The probability of detection of a GWB vs. further observing time for a PTA made up of the best 4 pulsars of the PPTA (Shannon et al. 2015), an augmented NANOGrav (current array plus 4 new  $\sigma_n = 250$  ns pulsars per year), an augmented IPTA (6 new  $\sigma_n = 250$  ns pulsars per year), and a theoretical PTA, consisting of 50 pulsars each with  $\sigma_n = 100$  ns and no intrinsic timing noise. The GWB amplitude distribution of Sesana (2013b) was used, on top of which various astrophysical effects were considered: blue and red lines show zero and 90% of binaries stalled, respectively. Dashed lines correspond to the case where the true background spectrum has a turn-over at  $f = 1/(11\text{y})$  due to binary environmental coupling.

### 4.3. PTA optimization

Should we spend our time observing a few wisely-chosen pulsars, or should we observe as many as possible that can reach a fixed  $\sigma_n$  limit? This debate remains a somewhat contentious topic, as its answer depends keenly on the severity of (unknown) levels of long-term intrinsic timing noise, on the type of target one is interested in, and on whether one is aiming for simply detection, or also extensive GW source characterization (Lommen 2012; Burt, Lommen & Finn 2011; Christy et al. 2014). For instance, any PTA aimed at GW detection should spend intensive time observing their few lowest- $\sigma_n$  pulsars (Lee et al. 2012). However, this optimization scheme is risky if intrinsic red noise dominates these pulsars over the long term; sensitivity to low-frequency signals like the GWB may be lost, thus arguing for long-term programs on large numbers of pulsars. Likewise, localization and characterization of a discrete GW source benefits from a large array of pulsars well-distributed on the sky. Some guidance on this topic comes from the prediction that the GWB will be discovered first (with a probability of  $\sim 70\text{-}90\%$ ; Rosado, Sesana & Gair 2015). However, both cosmic variance and long-term science should also be considered.

### 4.4. Time to detection

The question of “when will we detect GWs” confronts a vast range of uncertainties which we review here. The anticipated time to detection depends most prominently on the strength of the expected signals, but also depends heavily on the number of pulsars available with low  $\sigma_n$  that are used in an array (§4.2), on the total observing span of the experiment, and on the prevalence of intrinsic red noise in pulsars’ spin variations, which can dampen PTAs’ sensitivity to low-frequency signals. Cutler et al. (2014) derived a generic S/N scaling for any signal of known shape in the case of white-dominant and red-dominant timing noise (see their Eq. 2.1 and 2.7, respectively).

Siemens et al. (2013) demonstrated that scaling laws differ in the weak, intermediate, and strong GW signal regimes, and used these scalings—coupled with predictions of new pulsar discoveries and varying levels of white and red noise—to predict when the NANOGrav timing array might

make its first detection of a power-law GWB from BSMBHs (however, it is not clear that the GWB will be a power-law; see Fig. 10). The result of that analysis, coupled most recent GWB limit (Shannon et al. 2015) of  $A_{1\text{yr}} < 1.0 \times 10^{-15}$ , indicates that for NANOGrav the earliest expected detection of the GWB could be between 2019 and 2023, barring the most pessimistic red noise scenario explored by Siemens et al. (2013).

Taylor et al. (2015a) explored the impact of BSMBH stalling and environment on the time to detection of a GWB (§5.2), as shown in Fig. 9. They demonstrate that the expected detection dates will be accelerated with the full IPTA, which can provide immediate access to longer data sets with several low- $\sigma_n$  pulsars. The time to detection will be pushed further into the future if there is a low-frequency turn-over in the GWB (§5), although the expected delay in detection due to a turn-over might only be up to  $\sim 2\text{-}3$  years. Importantly, Fig. 9 demonstrates how while timing only a few high-precision pulsars may place strict limits on the GWB, a confident detection can only be achieved by timing a large array of pulsars.

Finally, note that it may also be that a turn-over in the GWB spectrum would make the detection of CWs more likely in the near-term, despite delaying a GWB detection; this possibility has yet to be explored.

### 4.5. Anisotropy of the sky

Until recently, a simplifying assumption had been made that the GWB is formed by a smooth distribution of sources. Now under consideration is whether the sky could in fact have an anisotropic distribution. In this case, one or several discrete GW sources that are *not* resolvable from the background could induce greater GW power in the background than other areas of sky (e.g. Ravi et al. 2012). Such might be expected from the natural large-scale clustering in a hierarchically built Universe (e.g. Simon et al. 2014). Accordingly, methods to limit, detect, and characterize an anisotropic background are being developed (Mingarelli et al. 2013; Taylor et al. 2015c).

## 5. Advances in Structure Formation

As seen by their starring role in §3 and Figs. 5–7, BSMBHs are the brightest anticipated GW

source in the PTA band. BSMBHs are formed during the merger of two massive galaxies, and these facts together decisively bind PTA detection of GWs to studies of galaxy evolution and structure formation in the Universe.

Generally the most massive, nearby pairs should form the dominant contribution to PTA-detectable signals. That is, binary systems with redshift  $z \lesssim 2$  and chirp mass  $M_c > 10^8 M_\odot$  (Sesana, Vecchio & Colacino 2008). Chirp mass is defined for a binary with masses  $m_{\bullet 1}$  and  $m_{\bullet 2}$  as  $M_c = (m_{\bullet 1} m_{\bullet 2})^{3/5} / (m_{\bullet 1} + m_{\bullet 2})^{1/5}$ .

Direct constraints on BSMBH demographics are far from robust, because only a handful of candidate BSMBH systems have been identified. Accordingly, GW predictions are based on theoretical and observational constraints on the evolution of SMBH host galaxies.

As a result of this, GW predictions show a broad range in strength and frequency distribution. In this section we paint a picture of how galaxy evolution is thus decisively a PTA science.

### 5.1. Building gravitational waves

The GWB from BSMBHs is simply the square strain integrated over all discrete BSMBH systems:

$$h_c^2(f_r) = \int \int \int \frac{dN_\bullet}{dz dm_{\bullet 1} dq_\bullet d(\ln f)} \times h_s(m_{\bullet 1}, q, z, f)^2 dz dm_{\bullet 1} dq_\bullet, \quad (6)$$

here posed as the integration over the differential number of BSMBHs  $N_\bullet$  per mass, mass ratio  $q$ , redshift, and logarithmic frequency interval (e.g. Sesana, Vecchio & Colacino 2008). The rotation and sky-averaged strain of a discrete source is

$$h_s = \sqrt{\frac{32}{5}} (\pi f_r)^{2/3} \frac{(GM_c)^{5/3}}{c^4 D}, \quad (7)$$

(e.g. Peters & Mathews 1963) where  $D$  is the proper (co-moving) distance to the binary.

As previously noted, there is no way to directly measure the distribution of BSMBHs in  $z$ ,  $m_{\bullet 1}$ , and  $q_\bullet$ , however we can measure the properties of SMBH host galaxies. Thus the *galaxy* distribution,  $dn/(dz dM dq)$ , is produced as a proxy. Subsequently, galaxies in that distribution are populated with SMBHs to then form  $h_c(f)$ . This can

be done via the application of any of the empirical relations that tie black hole mass to host galaxy properties ( $M_\bullet$  with bulge mass, stellar velocity dispersion, etc., e.g. Magorrian et al. 1998; Ferrarese & Merritt 2000)

In early work, predictions were derived from numerical dark matter simulations and semi-analytic prescriptions to infer galaxy and SMBH evolution properties (Jaffe & Backer 2003; Wyithe & Loeb 2003; Enoki et al. 2004; Sesana et al. 2004; Sesana, Vecchio & Colacino 2008). Recent work, however, has focused on using the *observed* demographics of the  $z \lesssim 3$  galaxies that should host SMBHs, to directly infer the expected GWB and CW signals from supermassive binaries (see, e.g., Sesana 2013b; Ravi et al. 2015; Simon & Burke-Spolaor 2015). The number density of galaxy mergers is formed by combining the galaxy mass function at redshift  $z$ ,  $\phi(M, z)$ , with the galaxy merger rate; this expression can be constructed as

$$\frac{dn}{dz dM dq} = \Phi(M, z) \frac{\mathcal{F}(z, M, q) dt_r}{\tau(z, M, q) dz}, \quad (8)$$

where  $\mathcal{F}$  is the pair fraction of galaxies, and  $\tau$  is the typical merger timescale for a galaxy pair (e.g. a dynamical friction timescale). The factor  $dt_r/dz$  converts the proper time rate into a redshift rate. The parameters  $\phi$  and  $\mathcal{F}$  are observables, but  $\tau$  is typically estimated from numerical simulations of galaxy mergers (Sesana 2013b).

### 5.2. The effect of unknowns

The previous section outlined how the parameters of galaxy evolution relate to PTA measurements of GWs. An added layer of complexity for predicting GW signals from the BSMBH population is a binary's evolutionary path after its host galaxies merge. The basic process is that the SMBHs are first drawn to the merger's center via dynamical friction, form a wide binary and undergo three-body interactions with stars, after which other processes dissipate enough angular momentum for the binary to efficiently evolve to coalescence via gravitational radiation (Begelman, Blandford & Rees 1980). If no other processes dissipate the system's energy in the second to last stage, the binary may "stall," enduring a gigayears-long wait before entering the PTA band. On the other hand, three-body interactions and other effects such as gas inflow (Mayer et al. 2007)

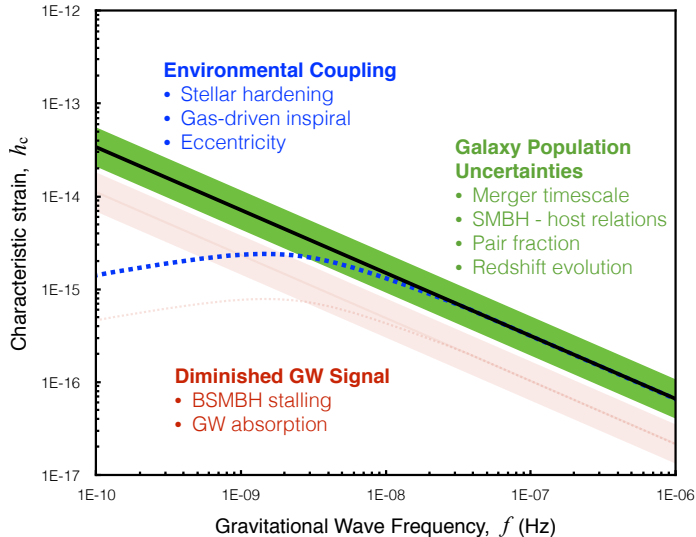


Fig. 10.— A conceptual view of how various uncertainties in the BSMBH population and the GWs we can detect from them can influence the amplitude and shape of the GWB. The line gives the mean of the power-law spectrum of Sesana (2013b), while the range shows the 68% range of power-law amplitude predictions based on the variance in observational limits on SMBH host galaxy properties. See §5.2 for a discussion of the effects shown in this figure.

may be so efficient that the binary is not purely driven by GWs through the nHz- $\mu$ Hz band, hence changing the expected form of the GW signal. Figures 1 and 10 show how such “super-efficient evolution” could make the expected GWB deviate from a simple power-law at low frequency (see also Enoki & Nagashima 2007; Kocsis & Sesana 2011; Sesana 2013a; McWilliams, Ostriker & Pretorius 2014; Ravi et al. 2014).

Recent efforts have broken down how uncertainties in galaxy and BSMBH evolution effect GW signals (Ravi et al. 2015; Simon & Burke-Spolaor 2015; Shannon et al. 2015). A conceptual view of the influence of various uncertainties is shown in Figure 10. The below factors are noted approximately in the order of what have the most to least amount of influence on GW signals (strength, rate of occurrence, and form) in the PTA band:

- **Effect of environment on BSMBH evolution:** As described above, we have basically no observational data on how BSMBHs couple with their environment during their evolution on scales of  $\lesssim 10$  pc. This is the most significant wildcard in GW predictions, although it is only expected to affect the low-

est frequencies,  $f \lesssim 10^{-8}$  Hz.

- **BSMBH stalling**, as a counter to the previous point, is essentially caused by the non-interaction of the BSMBH with its environment, leading to an exceptionally long time spent at separations  $\sim 0.1$ –10 pc. Long stalling times can potentially cause a large drop in the overall amplitude of the GWB, directly lowering the total number of BSMBHs contributing to the  $dN_{\bullet}/d(\dots)$  term in Eq. 6.
- **Eccentricity** redistributes power to higher harmonics in GW frequency and changes the waveform of a CW. If eccentricity is common it would increase the complexity of CW searches, although may raise the probability of CW detection over that of GWB detection (Taylor et al. 2015b; Huerta et al. 2015). It may also raise the expected rate of bursts, although that has not yet been investigated. Unless all BSMBH systems are driven by environments to extreme orbits ( $e \gtrsim 0.9$ ), the GWB strength will be diminished, but not by much (Enoki & Nagashima 2007; Ravi et al. 2014; Huerta et al. 2015).

- **Merger timescale**,  $\tau$ , was shown by Ravi et al. (2015) to be the most significant contributor to variance in  $A_{1\text{yr}}$  predictions; the range of theoretical estimations for this parameter vary by a large factor (e. g. Kitzbichler & White 2008; Lotz et al. 2011).
- **SMBH-host galaxy relations and their redshift evolution** are used to cast galaxy properties to the BSMBH properties used in GW simulations. Measurement error and intrinsic scatter in these vary the GW predictions, however the most significant issues are a) the deficit of direct SMBH measurements at high redshift that forbid a measurement of the redshift-dependence, and b) the deficit of measurements of the highest-mass SMBHs which would contribute most strongly to PTA-detectable signals.
- **GW-diminishing effects**: Finally, it has been noted that there may be several other, more exotic, causes of a diminished GW signal. Shannon et al. (2015) suggested that their limit was consistent with “GW absorption” to other matter in the Universe; while according to Hawking (1966) this could in principle occur, our current knowledge of cosmological constants imply that in our expanding Universe this should not be the case, as the mean free path is much greater than the GW wavelength, particularly at the redshifts  $z \lesssim 3$  from which we expect the majority of contributing GW signals from BSMBH systems. If gravity instead follows one of many non-general-relativistic theories, this could in principle change the expected signal, although the effect of these on the GWB has not been investigated.

Measurement uncertainties in galaxy stellar mass functions and pair fractions appear to contribute relatively little to the variance in GWB simulations (Ravi et al. 2015; Simon & Burke-Spolaor 2015).

### 5.3. What PTAs can address

Most fundamentally, PTAs are able to limit or measure GW power as a function of frequency. Studies of galaxy mergers and evolution provide

constraints on many, but not all, of the constituents of Eq. 6. Thus, PTAs can infer limits on the unknowns detailed in the previous section. Here we highlight a few recent results that provide examples of how PTA science is impacting galaxy evolution.<sup>8</sup>

In the basic assumption of a power-law background (Eq. 4), Simon & Burke-Spolaor (2015) mapped PTA limits directly to limits on the slope, intercept, and intrinsic scatter of the  $M_{\bullet}$ - $M_{\text{bulge}}$  relation. The PTA limits of Shannon et al. (2015) were discrepant with some  $M_{\bullet}$ - $M_{\text{bulge}}$  measurements. Simon & Burke-Spolaor thus demonstrated that BSMBH inspirals stalling on average timescales of  $> 0.73$  Gyrs could solve this discrepancy.

Employing Bayesian evidence techniques, Arzoumanian et al. (2015a) determined that their limit on BSMBHs favors a low-frequency turn-over over a pure power-law spectrum with an odds ratio of 2.2:1 for the model of Sesana (2013b). This is a model which aimed to estimate the full range of uncertainties in our knowledge of galaxy evolution. That is, if other GW-diminishing effects are not influential (Fig. 10), the Arzoumanian et al. limit has shown that environmental factors do appear to be influencing the binary at frequencies  $\lesssim 10^{-8}$  Hz. This work went on to demonstrate how the turn-over frequency of the spectrum can be mapped to the mass density of stars in the galactic core, the accretion rate of the primary black hole from a circumbinary disk, and/or the eccentricity of a BSMBH at binary formation.

Similarly, Shannon et al. (2015) interpreted their limit as favoring either stalled BSMBHs or strong environmental interactions, as their upper limit—the most stringent to date, of  $A_{1\text{yr}} < 1.0 \times 10^{-15}$ —rules out the majority of simplistic power-law models that take into account neither stalling nor environmental coupling.

## 6. Multi-messenger detection

“Multi-messenger detection” refers to the detection of an object in both electromagnetic and non-electromagnetic emission. This is a particu-

<sup>8</sup>PTAs can limit BMSBH merger densities as a function of mass without any external assumptions or inputs, however these limits are not strongly constraining (Middleton et al. 2015).

larly attractive venture as it would open up novel studies of extreme-gravity systems, providing access to physical and astrophysical studies beyond those which could be done with GW or electromagnetic emission detection alone. In addition, like the galaxy evolution studies described in the previous section, this is another symbiotic PTA science; an electromagnetic detection of a BSMBH’s periodicity within the nHz- $\mu$ Hz band could raise the signal-to-noise ratio of a CW by  $\geq 30\%$  (Ellis & Burke-Spolaor 2014), potentially enabling a confident GW detection of that binary. On the other hand, a CW detection reported by PTAs would provide surveyers a targeted swath of sky in which to perform a deep search for a system of relatively well-constrained period, distance, and mass (Ellis 2013).

Considering a BSMBH, multi-messenger emission with PTAs would need an electromagnetic marker of a coalescence event for memory, or of a weeks- to decades-period BSMBH for CW detection. Burke-Spolaor (2013) and Schnittman (2013) provide recent reviews of the gamut of electromagnetic emissions that may accompany PTA targets.

There are extensive ongoing efforts to identify BSMBHs at nearly all electromagnetic wavebands (see e.g. Rodriguez et al. 2006; Eracleous et al. 2012; Burke-Spolaor 2011; Graham et al. 2015a, for only a few of many examples in the past two decades). Some candidates have been identified that lie in the nHz- $\mu$ Hz band (e.g. Valtonen et al. 2011; Graham et al. 2015b; Liu et al. 2015), however none since 3C66B have been expected to be detectable by PTAs.

## 7. Conclusions

We have summarized the current status of gravitational wave detection with pulsar timing array experiments, and hope to have impressed the extremely broad range in science and expertise that this field involves.

We would like to close with a few concluding thoughts from this review:

**Pulsar timing forms a competitive and complementary method of gravitational wave detection.** The earliest expected detection could arise in just a few years (§4.4), and PTAs’ target gravitational waveband and source popula-

tions are complementary to those of space-based and ground-based GW experiments (Fig. 1).

**Supermassive black hole binaries are likely to be PTAs’ dominant target signal,** exceeding the waves expected from other sources like cosmic strings and inflationary GWs. This includes sensitivity to bursting and continuous GW sources, as well as memory events and an ensemble background (§3).

**PTAs science is Galaxy Evolution and Binary Supermassive Black Hole science.** As PTAs are cutting into the predicted GWB from BSMBHs, we are beginning to understand how to map GW upper limits directly to limits on the properties of the BSMBH population and their host galaxies (§5). While PTAs can not currently decouple all the parameters, further observational constraints on the galaxy population—as well as the discovery and study of BSMBHs in the gravitational wave regime (§6), which will reveal their eccentricities and how efficiently these systems evolve—will lead to tight characterization of the BSMBH population.

**PTA sensitivity to GWs is impacted by radio telescope sensitivity, the limited number of known good timing pulsars, and timing noise.** Future telescopes like FAST and the SKA will greatly improve our sensitivity by providing high S/N detections of good timers, as well as probing deeper into our Galaxy to find a large number of PTA-contributing pulsars. The increasing-at-low-frequency red noise exhibited by some timing pulsars (§4.1) can cause significant sensitivity issues for long-term ( $> 10$  yr) experiments, however by adding more pulsars to an array, red noise might not have a strong impact on our time to detection (§4.4).

**PTAs are much more than great astrophysics.** Although we did not review non-GW science in this review, pulsar timing contributes fundamentally to other areas of study that we encourage the reader to explore. We briefly mentioned fundamental gravity tests in §3.1; PTAs have also been used to measure terrestrial time standards (Hobbs et al. 2012) and planetary masses (Champion et al. 2010). X-ray timing has also been proposed for use in autonomous spacecraft navigation systems (Li & Ke 2009).

In conclusion, in the coming years the ongoing



timing of pulsars and contributions from new telescopes will rapidly drive PTA science from “beginning to impact our knowledge of the Universe” to “measuring the structure and evolution of the Universe.”

The TEMPO2 pulsar timing software package was used to generate and analyse data for this paper (Hobbs et al. 2009). We thank Stefan Osłowski for directing us to single-pulse data from PSR J0437–4715. The National Radio Astronomy Observatory is a facility of the National Science Foundation operated under cooperative agreement by Associated Universities, Inc.

## REFERENCES

- Arzoumanian Z. et al., 2015a, arXiv:1508.03024
- Arzoumanian Z. et al., 2015b, arXiv:1505.07540
- Arzoumanian Z. et al., 2015c, arXiv:1501.05343
- Arzoumanian Z. et al., 2014, ApJ, 794, 141
- Backer D. C., Kulkarni S. R., Heiles C., Davis M. M., Goss W. M., 1982, Nature, 300, 615
- Backer D. C., Kulkarni S. R., Taylor J. H., 1983, Nature, 301, 314
- Barr E. D. et al., 2013, MNRAS, 429, 1633
- Bates S. D. et al., 2015, MNRAS, 446, 4019
- Begelman M. C., Blandford R. D., Rees M. J., 1980, Nature, 287, 307
- Blandford R., Romani R. W., Narayan R., 1984, Journal of Astrophysics and Astronomy, 5, 369
- Boyle L., Pen U.-L., 2012, Phys. Rev. D, 86, 124028
- Bugaev E., Klimai P., 2011, Phys. Rev. D, 83, 083521
- Burke-Spolaor S., 2011, MNRAS, 410, 2113
- Burke-Spolaor S., 2013, Classical and Quantum Gravity, 30, 224013
- Burt B. J., Lommen A. N., Finn L. S., 2011, ApJ, 730, 17
- Caprini C., Durrer R., Siemens X., 2010, Phys. Rev. D, 82, 063511
- Chamberlin S. J., Siemens X., 2012, Phys. Rev. D, 85, 082001
- Champion D. J. et al., 2010, ApJ, 720, L201
- Christy B., Anella R., Lommen A., Finn L. S., Camuccio R., Handzo E., 2014, ApJ, 794, 163
- Cordes J. M., 2013, Classical and Quantum Gravity, 30, 224002
- Cordes J. M., Jenet F. A., 2012, ApJ, 752, 54
- Cornish N. J., 2012, arXiv:1209.6428
- Cutler C., Burke-Spolaor S., Vallisneri M., Lazio J., Majid W., 2014, Phys. Rev. D, 89, 042003
- Damour T., Vilenkin A., 2001, Phys. Rev. D, 64, 064008
- Demorest P. B., Ferdman R. D., Gonzalez M. E., et al., 2013, ApJ, 762, 94
- Deng X., 2014, Phys. Rev. D, 90, 024020
- Detweiler S., 1979, ApJ, 234, 1100
- Ellis J., Burke-Spolaor S., 2014, in American Astronomical Society Meeting Abstracts, Vol. 223, American Astronomical Society Meeting Abstracts #223, p. #429.04
- Ellis J., Siemens X., Chamberlin S., 2012, arXiv:1210.5274
- Ellis J. A., 2013, Classical and Quantum Gravity, 30, 224004
- Ellis J. A., Siemens X., van Haasteren R., 2013, ApJ, 769, 63
- Enoki M., Inoue K. T., Nagashima M., Sugiyama N., 2004, ApJ, 615, 19
- Enoki M., Nagashima M., 2007, Progress of Theoretical Physics, 117, 241
- Eracleous M., Boroson T. A., Halpern J. P., Liu J., 2012, ApJS, 201, 23
- Favata M., 2009a, ApJ, 696, L159
- Favata M., 2009b, Phys. Rev. D, 80, 024002

- Ferrarese L., Merritt D., 2000, *ApJ*, 539, L9
- Finn L. S., Larson S. L., Romano J. D., 2009, *Phys. Rev. D*, 79, 062003
- Finn L. S., Lommen A. N., 2010, *ApJ*, 718, 1400
- Graham M. J. et al., 2015a, *MNRAS*, 453, 1562
- Graham M. J. et al., 2015b, *Nature*, 518, 74
- Grishchuk L. P., 2005, *Physics Uspekhi*, 48, 1235
- Hawking S. W., 1966, *ApJ*, 145, 544
- Hellings R. W., Downs G. S., 1983, *ApJ*, 265, L39
- Hobbs G. et al., 2010, *Classical and Quantum Gravity*, 27, 084013
- Hobbs G. et al., 2012, *MNRAS*, 427, 2780
- Hobbs G., Dai S., Manchester R. N., Shannon R. M., Kerr M., Lee K. J., Xu R., 2014, *ArXiv e-prints*
- Hobbs G. et al., 2009, *MNRAS*, 394, 1945
- Huerta E. A., McWilliams S. T., Gair J. R., Taylor S. R., 2015, *Phys. Rev. D*, 92, 063010
- Jaffe A. H., Backer D. C., 2003, *ApJ*, 583, 616
- Janssen G. et al., 2015, *Advancing Astrophysics with the Square Kilometre Array (AASKA14)*, 37
- Jenet F. A., Armstrong J. W., Tinto M., 2011, *Phys. Rev. D*, 83, 081301
- Jenet F. A., Creighton T., Lommen A., 2005, *ApJ*, 627, L125
- Jenet F. A. et al., 2006, *ApJ*, 653, 1571
- Jenet F. A., Lommen A., Larson S. L., Wen L., 2004, *ApJ*, 606, 799
- Kaspi V. M., Taylor J. H., Ryba M. F., 1994, *ApJ*, 428, 713
- Kitzbichler M. G., White S. D. M., 2008, *MNRAS*, 391, 1489
- Kocsis B., Sesana A., 2011, *MNRAS*, 411, 1467
- Kramer M., Champion D. J., 2013, *Classical and Quantum Gravity*, 30, 224009
- Lee K. J., Bassa C. G., Janssen G. H., Karuppusamy R., Kramer M., Smits R., Stappers B. W., 2012, *MNRAS*, 423, 2642
- Lee K. J., Wex N., Kramer M., Stappers B. W., Bassa C. G., Janssen G. H., Karuppusamy R., Smits R., 2011, *MNRAS*, 414, 3251
- Lentati L. et al., 2015, *arXiv:1504.03692*
- Li J., Ke X., 2009, *Science in China: Physics, Mechanics and Astronomy*, 52, 303
- Liu T. et al., 2015, *ApJ*, 803, L16
- Lommen A. N., 2001, PhD thesis, University of California, Berkeley
- Lommen A. N., 2012, *Journal of Physics Conference Series*, 363, 012029
- Lommen A. N., Backer D. C., 2001, *ApJ*, 562, 297
- Lorimer D. R., Kramer M., 2004, *Handbook of Pulsar Astronomy*
- Lotz J. M., Jonsson P., Cox T. J., Croton D., Primack J. R., Somerville R. S., Stewart K., 2011, *ApJ*, 742, 103
- Lynch R. S. et al., 2013, *ApJ*, 763, 81
- Madison D. R., Cordes J. M., Chatterjee S., 2014, *ApJ*, 788, 141
- Maggiore M., 2000, *Phys. Rep.*, 331, 283
- Magorrian J. et al., 1998, *AJ*, 115, 2285
- Manchester R. N. et al., 2013, *PASA*, 30, 17
- Manchester R. N., IPTA, 2013, *Classical and Quantum Gravity*, 30, 224010
- Mayer L., Kazantzidis S., Madau P., Colpi M., Quinn T., Wadsley J., 2007, *Science*, 316, 1874
- McHugh M. P., Zalamansky G., Vernotte F., Lantz E., 1996, *Phys. Rev. D*, 54, 5993
- McLaughlin M., 2014, *General Relativity and Gravitation*, 46
- McLaughlin M. A., 2013, *Classical and Quantum Gravity*, 30, 224008
- McWilliams S. T., Ostriker J. P., Pretorius F., 2014, *ApJ*, 789, 156

- Merritt D., Milosavljević M., 2005, *Living Reviews in Relativity*, 8, 8
- Middleton H., Del Pozzo W., Farr W. M., Sesana A., Vecchio A., 2015, *ArXiv e-prints*
- Mingarelli C. M. F., Sidery T., Mandel I., Vecchio A., 2013, *Phys. Rev. D*, 88, 062005
- Ölmez S., Mandic V., Siemens X., 2010, *Phys. Rev. D*, 81, 104028
- Ośłowski S., van Straten W., Hobbs G. B., Bailes M., Demorest P., 2011, *MNRAS*, 418, 1258
- Peters P. C., Mathews J., 1963, *Physical Review*, 131, 435
- Phinney E. S., 2001, *ArXiv Astrophysics e-prints*
- Ravi V., Wyithe J. S. B., Hobbs G., Shannon R. M., Manchester R. N., Yardley D. R. B., Keith M. J., 2012, *ApJ*, 761, 84
- Ravi V., Wyithe J. S. B., Shannon R. M., Hobbs G., 2015, *MNRAS*, 447, 2772
- Ravi V., Wyithe J. S. B., Shannon R. M., Hobbs G., Manchester R. N., 2014, *MNRAS*, 442, 56
- Rawley L. A., Taylor J. H., Davis M. M., Allan D. W., 1987, *Science*, 238, 761
- Rickett B. J., 1975, *ApJ*, 197, 185
- Rodriguez C., Taylor G. B., Zavala R. T., Peck A. B., Pollack L. K., Romani R. W., 2006, *ApJ*, 646, 49
- Rosado P. A., Sesana A., Gair J., 2015, *MNRAS*, 451, 2417
- Schnittman J. D., 2013, *Classical and Quantum Gravity*, 30, 244007
- Sesana A., 2013a, *Classical and Quantum Gravity*, 30, 224014
- Sesana A., 2013b, *MNRAS*, 433, L1
- Sesana A., Haardt F., Madau P., Volonteri M., 2004, *ApJ*, 611, 623
- Sesana A., Vecchio A., Colacino C. N., 2008, *MNRAS*, 390, 192
- Sesana A., Vecchio A., Volonteri M., 2009, *MNRAS*, 394, 2255
- Seto N., 2009, *MNRAS*, 400, L38
- Shannon R. M., Cordes J. M., 2012, *ApJ*, 761, 64
- Shannon R. M. et al., 2014, *MNRAS*, 443, 1463
- Shannon R. M. et al., 2013, *Science*, 342, 334
- Shannon R. M. et al., 2015, *ArXiv e-prints*
- Siemens X., Ellis J., Jenet F., Romano J. D., 2013, *Classical and Quantum Gravity*, 30, 224015
- Simon J., Burke-Spolaor S., 2015, *submitted*
- Simon J., Polin A., Lommen A., Stappers B., Finn L. S., Jenet F. A., Christy B., 2014, *ApJ*, 784, 60
- Stinebring D. R., Ryba M. F., Taylor J. H., Romani R. W., 1990, *Physical Review Letters*, 65, 285
- Sudou H., Iguchi S., Murata Y., Taniguchi Y., 2003, *Science*, 300, 1263
- Swiggum J. K. et al., 2014, *ApJ*, 787, 137
- Taylor S., Vallisneri M., Ellis J. A., Mingarelli C., Lazio T. J. W., van Haasteren R., 2015a, *submitted to ApJ Letters*
- Taylor S. R., Huerta E. A., Gair J. R., McWilliams S. T., 2015b, *ArXiv e-prints*
- Taylor S. R. et al., 2015c, *Physical Review Letters*, 115, 041101
- Valtonen M. J., Lehto H. J., Takalo L. O., Sillanpää A., 2011, *ApJ*, 729, 33
- van Haasteren R., Levin Y., 2010, *MNRAS*, 401, 2372
- van Haasteren R. et al., 2011, *MNRAS*, 414, 3117
- van Haasteren R., Mingarelli C. M. F., Vecchio A., Lasso A., 2013, *arXiv:1301.6673*
- Wang J. B. et al., 2015, *MNRAS*, 446, 1657
- Wyithe J. S. B., Loeb A., 2003, *ApJ*, 590, 691
- Zhao W., 2011, *Phys. Rev. D*, 83, 104021
- Zhu X.-J. et al., 2014, *MNRAS*, 444, 3709
- Zhu X.-J. et al., 2015, *MNRAS*, 449, 1650

---

This 2-column preprint was prepared with the AAS L<sup>A</sup>T<sub>E</sub>X macros v5.2.